Simulation of scree slope dynamics: Investigating the distribution of debris avalanche events in an idealised two dimensional model.

Mike Bithell

mb425@cam.ac.uk

+44(0)1223333361

Keith S. Richards

ksr10@cam.ac.uk

+44(0)1223766579

Department of Geography, University of Cambridge, Downing Place, Cambridge, CB2 3EN,UK

and

Erica G. Bithell

egb10@cam.ac.uk

+44(0)1223746249

Institute of Continuing Education, University of Cambridge, Madingley Hall, Cambridge, CB23 8AQ, UK

Published in Earth Surface Processes and Land Forms, **39**(12), 1601-1610, 2014

DOI:10.1002/esp.3548

Abstract

We present a two-dimensional model of the development of scree slopes using the discrete-element method. We concentrate on the dynamics of the accumulating debris at the cliff foot rather than on the failure modes of the cliff-face or shape of the underlying rock surface. The evolution of this unconsolidated material is intermittent and systematically changing over time, with an early high disturbance regime, dominated by a characteristic event size (where 65% of particles in the debris are in motion to some extent), replaced at later times by many shallow slides interspersed with infrequent large events that involve motion through almost the full scree depth. These large slides lead to a stratigraphy in which the layers of material are stretched almost horizontal near the base of the slope. The scree surface thus shows a gradient in age with most recent rock-fall close to the cliff and the oldest rock-fall debris outcropping at the foot. The final surface slope tends to show little curvature, and the final mean slope is well correlated with the angle of internal friction of the particles, although the change is very small over a wide range of friction angles (Final slope (in degrees relative to horizontal)~ 0.043*Internal Friction angle +17.49, with a Correlation coefficient of 0.89, p-value 0.0001). Some weak size-segregation of the debris is found, but this seems to have little to do with individual particles bounding down the slope. The shape of the rock core agrees largely with the analytic forms given by Fisher-Lehmann and Bakker LeHeux expressions, but the original simple Fisher quadratic can give the best fit. Overall the evolution shows a remarkable insensitivity to the model parameters, suggesting that the controls on dry scree-slope evolution are primarily geometric in character.

1) Introduction

In the 1860s the Reverend Osmond Fisher took a stroll to an old quarry near Lewes in Sussex and was inspired to develop a mathematical description of the evolution of the rock surface underlying a developing scree slope (Fisher 1866). He derived a simple quadratic form relating the vertical to the horizontal co-ordinates of the rock surface, with angle of repose of the scree material and cliff height as parameters. The model assumed that incremental recession of the cliff produced rock debris that spread uniformly across the surface of the scree accumulating at the foot of the cliff, implying a surface-parallel stratigraphy for scree sedimentation. This explanation has endured, with minor elaborations to allow for different porosity and volumetric increase in the debris and for varying effects of basal removal (Lehmann 1933; Bakker and Le Heux, 1947a,b, 1952a,b, Scheidegger 1961). However, the basic model of the rock profile has not been fundamentally challenged. Only relatively recently have numerical (Nash 1981, Utili and Crosta 2011), field (Caine 1969, Hutchinson 1998) and laboratory (DeBlasio and Saeter 2009) experiments sought to elaborate on these more mathematical studies. The laboratory data in particular imply that there is more to the dynamics than a simple equilibrium accumulation of material at the base of the cliff, suggesting that there is a dynamical evolution of the scree itself, in which the whole slope surface may periodically be involved in mass movements.

The suggestion of mass movement connects the question of the rock-head geometry to the evolution of the cliff-scree system as a whole, and to the dynamic relationship between rock-fall and scree-slope processes. These have been analysed both mathematically and experimentally (Kirkby and Statham 1975, Statham 1973,1976) with additional insights provided by Carson (1977). These papers emphasise the role of rock-fall, concluding that

the evolving scree morphology and sedimentology reflect the balance between rock-fall supply and shallow sliding. In particular, the momentum of rock-fall input was considered to result in scree surface slopes that are less than the angle of repose when the cliff is a high percentage of total slope height, but to a decreasing extent as this percentage diminishes (implying a convergence towards the angle of repose). In addition they argue that rock-fall results in significant scree profile concavity when the cliff is a large percentage of slope height, with a convergence to a straighter profile the more the scree encroaches up the slope. Related to this is a size sorting involving a downslope coarsening which arises because large individual boulders fail to find a depositional niche, and their input momentum allows them to bounce and roll to the foot of the scree. Finally, work on self-organised criticality suggests that scree surfaces close to the angle of repose may be subject to avalanches in the form of shallow translational landslides whose size distribution might follow some kind of power-law size-distribution (Bak et al 1987, but see comments in van Steijn 2002).

In this paper we model the dynamics of scree slope evolution in detail, by simulating the accumulation of debris directly using a discrete element model that tracks the dynamics of each rock particle after its fall from the cliff face. We do not attempt to examine the process by which the cliff itself disaggregates – Utili and Crosta (2011) have already made some progress on this front. Rather, we assume there is some weathering process that results in a given particle size distribution of fragments that fall more or less at random from the exposed cliff face, and we allow these to drop to the cliff foot where they interact with the loose material as it accumulates there. We will examine the distribution and timing of avalanche and sliding events, and their effects on the time evolution of the scree, and test the sensitivity of these results to model parameters.

2) The Discrete Element Method (DEM)

DEM is a particle-based simulation technique in which Newton's equations of motion are solved explicitly for every particle individually (Cundall 1971, Cundall and Strack 1979: see also Richards and Dove 2004 and papers therein, and the review by Bobet et al 2009). The use of the discrete element method has a number of advantages in relation to understanding of the cliff-scree system and its evolution. We are able to view the motion of the debris throughout its full depth, and to examine the velocity distribution of all the particles. Since the whole structure is visible and we can track every particle, we are able to view the development of size segregation and assess the mechanism by which this appears to take place: this is difficult to achieve with any other methodology. In addition, we are able to see the development of a stratigraphy within the debris, and predict where we would expect to see the most recent rock-fall material as a function of distance down the surface of the scree slope. Finally, we can, as a side effect, track the evolution of the underlying undisturbed rock surface, and compare this with the expected shape derived from analytic methods.

We sketch the method here to outline the parameters that are of relevance, but for more detail the reader is referred to the above references and to comprehensive descriptions that exist in the literature (see for example, Munjiza (2004)). In this paper we follow the method as laid out in Cleary and Prakash (2004). Suppose we have a set of particles for which we know mass m_i for each particle i, position vectors of the centre of mass, $\underline{x}_i$ and angular velocities $\underline{\omega}_i$. The particles are subject to body forces such as gravity, but other than this we assume that forces only act when particles are in contact, through elastic deformation of the particles during collsion, plus tangential frictional forces acting at the surface. So we can write

$$m_i \frac{\partial^2 \underline{x}_i}{\partial t^2} = \sum_j \underline{F}_{ij} + \underline{B}_i \qquad I_i \frac{\partial \underline{\omega}_i}{\partial t} = \sum_j \underline{T}_{ij} + \underline{R}_i$$

Where $\underline{F}_{ij}$ are the forces acting between particle i and j, and $\underline{B}_i$ are the body forces acting on the particle, including gravity. I_i is the particle moment of inertia, $\underline{T}_{ij}$ the torque between particle i and j and $\underline{R}_i$ any torque acting other than those due to particle interactions: we have assumed that the torques are expressed in the principle axes of each particle, so that we can use the principle moments of inertia to compute the changes in rotation. To go further we need to know the particle shape, since this determines whether particles can be in contact, plus an algorithm for detecting contacts, and a force-law for estimating the resulting inter-particle forces. In this work we will simplify things by assuming spherical particles. This makes contact finding simple, since we can just cover the domain with a grid and test neighbouring grid-cells to see whether distances between the particles they contain are smaller than the sum of their radii. For forces we assume that particles act as though they are linear springs damped with dash-pots: Overlap between two particles is used as a proxy for spring compression, with a normal restoring force dependent linearly on the degree of overlap, and a tangential spring is assumed to be stretched by relative motion of the two surfaces, up to a maximum beyond which slip occurs, so

Normal Force $$\underline{F}_{ij}^N = -k_{ij}\Delta\underline{x}_{ij} + N\underline{\Delta u}_{ij}$$

Tangential Force $$\underline{F}_{ij}^T = \min\left\{\mu\left|\underline{F}_{ij}^N\right|, \left|k'_{ij}\int \underline{\Delta v}_{ij}dt + D\underline{\Delta v}_{ij}\right|\right\}\hat{\underline{t}}$$

Where k_{ij} is the stiffness of the spring acting to repel the two particles (which may differ from the tangential value k'_{ij}) and $\Delta\underline{x}_{ij}$ the particle overlap (directed along the spheres' line of centres). $\underline{\Delta u}_{ij}$ is the normal component of the relative velocity and N a damping

constant. $\underline{\Delta v}_{ij}$ is the tangential component of the relative velocity, D a coefficient that damps the tangential spring and $\hat{\underline{t}}$ is a unit vector aligned along the direction of the tangential spring. The coefficient of friction, μ, expresses the maximum tangential force as being proportional to the normal force.

We use a relatively soft spring constant, k, that limits particle overlaps to a few percent of the radius, but contributes rather lower stiffness than might be expected for real rock particles. This latter condition allows for a longer time-step than would be the case for a more exact stiffness, since the time-step required for numerical stability scales as $(m/k)^{1/2}$ where m is a measure of the particle mass. In the present work we use a normal spring constant of $5x10^{7}$ Nm^{-1}, which necessitates a time-step of about $2x10^{-5}$ seconds. Run times are therefore relatively long, with each simulation taking 36 hours to complete (slower than a standard run-out simulation since the cliff face takes time to disintegrate). In the following we take the tangential spring constant to be half the normal spring constant. Values for μ were chosen corresponding to internal friction angles between 20° and 57.5°. As will be seen below, the final outcomes of the modelling prove to be rather insensitive to these friction angles, with the final angle of repose lying well below the higher values

Both normal and tangential springs are linearly damped by applying a damping coefficient to the relative particle velocities. For normal collisions this leads to a coefficient of restitution that parameterizes the dissipation that takes place between real particles. Utili and Crosta (2011) regard this as a purely numerical device to speed up convergence of simulations, but experiments with granite spheres suggest that rock fragments far from fracture have coefficients of restitution in the region of 0.8 (Durda et al 2011). On the other hand Cleary and Prakash (2004) use much lower values (0.3), whereas the run-out simulations of Calvetti et al (2000) suggest values very close to 1. Here we vary the

coefficient of restitution across the range from 0.1 to 0.9. Again, the results for the bulk of the scree appear to depend only rather weakly on this parameter. Tangential damping was varied as a fraction of the normal damping. .

The micro-scale model for the interaction between particles is ad-hoc (although very widely used): other force laws are possible (see e.g. Schäfer et al 1996), but here we just use multiple model runs study to look for any major sensitivities in parameter values for this simple case.

3) Expressions for the form of the underlying rock surface

We summarize here the analytic expressions for the form of the rock head, for later reference. Recall that Fisher's original discussion gave a very simple quadratic relation between original cliff height, scree angle of repose and the form of the rock surface, thus:

$$y^2 = 2.h.x.\tan\alpha \quad \text{eq. 1}$$

where h is the initial cliff height and α the angle of repose of the scree, y the vertical and x the horizontal co-ordinate of the rock surface. Lehmann extended these results to allow for an initial cliff face with angle different from the vertical, and to allow for the debris volume to differ from the original volume of weathered material obtaining the more complex relationship (Hutchinson 1998):

$$x = k(l+m)\ln[m/(m-y)] - ky \quad \text{eq. 2}$$

Where m=h/c, k=(a-ac-d)/c, l=bh/(a-ac-b), c=1-rock volume/debris volume, h is the cliff height, a=cot α, b=cot β , α is the angle of the debris slope to the horizontal and β is the initial angle of the cliff face to the horizontal.

Bakker and LeHeux further extended this to allow for a gradually increasing angle of the cliff face above the debris (using central recession). This results in:

$$x = ay - (a-b)y\left[\left(h^2 + (1-2c)y^2\right)/h^2\right]^{(c-1)/(1-2c)} \quad \text{eq. 3}$$

where the symbols are as for equation 2.

4) Experimental method

For simplicity, we simulate the disintegration of a cliff face using spheres confined to move in two dimensions. This helps to reduce the expense of the runs, although the two dimensional representation may miss some aspects of the dynamics (e.g. the spread of particles out into fan-shaped structures). The cliff is represented as a packed conglomerate of boulder-sized spheres; this is not intended to represent any particular rock type, but allows us to set the size-distribution of fragments into which the rock will disintegrate. The idea is that a weathering process of some kind causes the exposed rock surface to break up into particles with a fixed size distribution, and these then free-fall onto the material below. So the initial internal distribution of rock particles in our simulation implicitly represents the final distribution of rock fragments into which the cliff can break up, rather than indicating an internal rock structure. It should be noted that having a range of sizes in the model is important; models with identically-sized sets of particles tend to exhibit "crystallized" regions in which the particles settle into a regular array (see e.g. Dickinson et al 1989, Lacaze et al 2008).

The initial condition for the simulations consists of a vertical cliff face, bounded above and below by quasi-horizontal surfaces (Figure 1). In order to create the initial internal distribution of particles within the cliff consistent with the model dynamics, an initial simulation is run by dropping the particles into a vertical-sided box with a horizontal base. An internal vertical wall is also included that will later define the front face of the cliff. Particles are randomly distributed on both sides of the internal wall, but with just enough

to the right of the wall to form a single layer to define a rough horizontal surface to the right. To the left, enough particles are added to form the bulk of the cliff itself. Particles are initially separated by a small distance so that when dropped they quickly come to equilibrium at rest within the box. We can thus generate a number of different initial conditions, with an uneven ground surface to the right of the internal wall, and a near-horizontal upper surface to the cliff that retains some variability. The initial state of the cliff face is self-consistent with the dynamics, so that internal spring compression within the system just balances gravity (a change in the spring constant therefore requires a new computation of the initial conditions).

Once the initial particle distribution has come to rest, all particles within the cliff wall are locked in place by setting a flag that ensures their acceleration remains at zero. The internal wall is then removed, so that particles on the front face can “weather out” and fall to the lower surface. We simulate the weathering process by searching for particles in every time-step that are within the diameter of the largest particles of the exposed surfaces (upper horizontal surface and cliff-face), and allowing a random fraction of these to move by un-setting the locking flag, so that they feel the acceleration due to gravity. The result is that progressively more particles in the cliff become unstable, eventually fall, and then expose the region behind, which subsequently becomes close enough to the surface to 'weather out'. The effect of this parameterization is to give a form of scratch/ravelling failure (using Utili and Crosta's (2011) terminology), where individual particle falls dominate the evolution rather than bulk failure, and the evolution is transport rather than weathering limited. As a result the cliff retreats in a fashion that allows for some variability in the shape of the surface, including the creation of overhangs, and of an overall slope that deviates from the vertical. Lower parts of the cliff face become progressively protected from weathering by a layer of accumulated debris that distances

them from the free surface. We do not attempt to constrain the recession, either to the vertical or to any other plan (such as Bakker and LeHeux's central recession), but allow the face to develop via the internal dynamics of the model.

As a result of this set-up we acquire a further set of parameters, namely the probability per time-step of a particle near the surface becoming free to move, and a size distribution for the particles. We set the probability per 100000 time-steps to 0.1: this is a compromise between having very long and inefficient run-times (where most of the run is spent waiting for particles to fall), and dynamically realistic runs where the scree settles completely and is essentially unmoving for long periods. The effect of this setting is that the cliff disintegration is very much more rapid than the real situation. This is an inevitable consequence of our needing very short time-steps to ensure numerical stability: without the accelerated evolution we would never be able to develop any interesting structures. Except in the initial stages, though, there is generally time for the scree to relax to a state where most rocks are at rest in between rock fall events. Further, avalanche and collapse events in the scree itself are simulated as they would happen in real-time, with simulated velocities close to those expected in real rock movements. One test run was conducted with a much slower release rate, but the results were consistent with the runs at higher release rates and we will not discuss it further. Runs continue until there is no remaining exposed rock face. The size of the intial block is chosen so that this occurs just about the time when the scree slope reaches the full height of the cliff, at which point the evolution would in any case cease.

For the particle sizes, we assume radii in the range 15-30cm, but test a range of size distributions. The initial height of the cliff (45m – see fig. 1) is thus about 75 times the diameter of the largest particles. Runs were undertaken with a uniform size distribution; and with two power-law distributions. One of these had particle numbers scaling as the

inverse of their radii, and the other had numbers scaling as the inverse of the radius cubed (i.e. equal masses in each particle size range). Particle density was assumed to be constant at 2500kg m^{-3}, although some test runs with much higher densities showed that the density made little difference to the outcome. These values for size, size distribution and density are not intended to be definitive, but simply representative of roughly realistic characteristics that might be encountered in real situations (see e.g. Sass 2006). The results presented here are taken from 384 runs of the model with parameters set as in Table 1. Thirty two repeats were made with each of 12 parameter sets, using a different sequence of pseudo-random numbers to determine the timing of rock falls in each of the thirty two runs. We can thus compare the variability in the results arising from random perturbations in the rock-fall with any systematic changes caused by internal friction angle or coefficient of restitution.

5) Results

A typical simulation initially shows a roughly triangular wedge of scree building at the base of the cliff. In the early stages, its geometry is highly dynamic as particles with a wide range of fall heights and kinetic energies impact on it; it can develop a convex surface profile that then collapses under impact. Some particles bounce across the scree and come to rest on the flat basal surface. As the scree grows, it buries the base of the cliff, and a curved bedrock profile develops as predicted by the Fisher-Lehmann-Bakker-Le Heux models. With the scree length and depth increasing, the maximum fall height from the cliff decreases, and the supply of material per unit time slows. The scree dynamics become more influenced by surface slides that redistribute debris that accumulates near the top of the scree; some of these failures are large and extend to the foot of the scree. Here, we extract some of the statistical properties that define the developing scree geometry and sedimentology, analyse and present them, and compare them both with the

previous analytical models and with typical field characteristics of scree slopes.

5.1)Frequency distributions of avalanches

In Figure 2 we show the time series of avalanching events for three model runs with different internal friction angles. We plot the number of particles in the moveable debris at the foot of the cliff for which velocities lie in the range 0.05m s^{-1} to 2m s^{-1} and for which vertical bins of width 2m contain at least 20 particles, excluding particles actively falling from the cliff. Time units here and in the plots below are "output steps" where model output was recorded after every 10000 model steps (with a time-step of $2.x10^{-5}$ seconds this means output steps are nominally 0.2 seconds long, but as we note above this is much speeded up compared with long-term real evolution of the scree, although it will capture the dynamics of *avalanches* in real-time). The plots show an early phase of gradually increasing avalanche size up to about output step 1000: during this time there is little coherent structure at the cliff base. Following this and up to output step of about 2000 the scree is relatively small and the input energy of rockfalls is high; in this regime particles are able to fall or bound down the full length of the debris slope, and have enough energy to disturb a large fraction of the material (a simple calculation suggests that, for the parameters we have here, the energy of rock fall is about the same as the stored potential energy in the scree as long as the scree depth is less than 10% of the cliff height). Mass movement events in the scree material are characterised by being of rather large size as a fraction of the total moveable debris, with the characteristic fraction in motion being of order 0.65. This is followed by a second regime as the scree grows and the input energy falls; particles dropping onto the surface are in general no longer able to run the full scree length, but instead are confined to a steadily smaller region close to the cliff, resulting in a gradual build-up of particles in the upper part of the scree. A series of small shallow avalanches re-distributes these particles for a while, but eventually a sufficient number

builds up to cause a large release of potential energy in which the scree becomes mobile through nearly the full depth and all the way to the base of the slope. Note that it is not the shallow slides per se that de-stabilise the whole system, but that the continual addition of material in the upper reaches of the debris leads to a bulk state that is only meta-stable, since the coupling between particles can transmit stress increases throughout the depth of the loose material. However the motion is generally quite slow except in the very surface layers (see figure 4).

As the evolution progresses the large events gradually decrease in frequency. The biggest, however, often occur when the upper portion of remaining exposed cliff is only a small fraction of the total slope height, near the end of the scree's development. Events involving moving particles (excluding very small events with fewer than 0.05% of the total number of particles in the scree moving) were identified in a time series of the fraction of scree in motion in a sliding window of width 20 output steps, and the peak value of the fraction moving was recorded for each window.

Figure 3 shows the resulting distributions of event sizes for the early part of the runs (output step < 1500, Fig. 3a) and the later part (output step >= 1500, Fig. 3b). We plot the mean number of events of a given size for each run set, with the standard deviation included for one set – other standard deviations are omitted for clarity, but are of similar magnitude. In the early part of the evolution there seems to be a characteristic event size, with a rather negatively-skewed distribution peaking between 0.6 and 0.7, followed by a sharply decreasing tail. The form of the distribution shows little systematic variation with the model parameters, except for the size of the peak of the distribution, which correlates well with the coefficient of restitution (Figure 3c). In this part of the run, since the disturbance is dominated by rock fall, it seems the damping afforded by lower coefficients of restitution helps to suppress the number of large events a little. This contrasts sharply

with the distribution of events at later times – then, the distribution is very broad and dominated by small events, but with a long tail out to very large sizes. The dynamics are now dominated by sliding events rather than fall of debris, and show almost no sensitivity to model parameters.

5.2)Internal structure

Figure 4 further illustrates the motion of the material during a large event (at step 4763 on Fig. 2b). Here the solid rock surface is shown in grey. Mobile material is coloured according to the speed of motion. The high velocity region visible near to the surface is highly transient and moves rapidly and intermittently across the upper part of the slope, but trending generally downward. Mostly speeds in excess of 0.8 m/s are confined to the upper part of the debris, but occasionally fingers of high velocity penetrate deeper into the particle mass, presumably following lines of higher than average stress (see e.g Brockbank et al 1997, Luding 1997, Makse et al 2000, Tuzun et al 2004, Utili and Crosta 2011). In the case of figure 4 the high speed finger is associated with the collapse of a void in the interior the talus (which was located just about the point of the highest speed particle, coloured red, near the end of the finger).

Below the surface high speed region there is a gentle velocity shear with alignment rather near to parallel with the upper scree surface. In the lower left part of the scree the very dark colours show the typically very low speeds in the protected region near the nose of the rock face. This material does not remain completely immobile, but moves very little by comparison with the upper layers, where velocities can reach as high as 2m s^{-1}, close to the reported typical speeds in dry grain flows (Sass and Krautblatter 2007). Note, however, that the mean speed of the moving fraction is lower (0.4 m/s at the time shown in figure 4, for example) One consequence of the continual occurrence of large avalanches, apart from exposure of fresh material in the upper rock face, is a re-orientation of the scree

material into nearly horizontal bands, with the material that fell from the cliff earliest sheared out to cover the whole length of the lowest part of the scree. This, combined with the fact that the particles falling from the cliff do not seem to bounce all the way to the scree foot, leads to a stratigraphy in which the earliest weathered material lies exposed at the base of the scree, with a gradient along the surface from the scree foot to the most newly-weathered material at the top. Figure 5 illustrates this by showing the later stages of run-set 9 run 7. In the very upper part of the scree the material is largely from recent rock falls, and is oriented more nearly parallel to the underlying surface, as it has not had the opportunity to be sheared like the lower layers. This material is confined to the upper part of the scree, as the motion of most rocks falling from the cliff is dissipated before they have managed to bounce more than part-way down the slope. The earlier weathered (light purple) material can clearly be seen extending in a band all the way from the underlying rock nose to the far end of the scree. A prediction of this model, therefore, is that one should find some of the earliest weathered rock closest to the scree base. By contrast, the incremental model in which the cliff material forms a layer lying along the whole surface of the scree would imply that the surface should be essentially uniform in age along the length of the scree, and should consist of the most recently weathered material.

5.3)Debris surface slopes

So far we have discussed the way in which the dynamics of the system evolves over time without much discussion of the shape of the resulting surfaces. In Figure 6 we show the time evolution of the upper exposed scree surface from set 9 run 27, with blue colours denoting early times and red colours later. In the early evolution there is a weak tendency for bench development at the top of the scree (asterisks), but this tends to be less pronounced later on. In the middle part of the evolution, there tend to be straighter slopes (plus signs). The non-uniformity of the evolution is reflected in the larger gaps between

earlier profiles of the scree, which builds vertically more rapidly in its early evolution because of its limited lateral extent, but later on experiences periods of relative quiescence as the supplied debris spreads over a longer surface, interspersed with surges of material transfer from up-slope. The non-monotonic evolution of the profile that results from this avalanching can be seen clearly in the latest profiles. The profile remains straight at output steps from 5000 to 6000, but the occurrence of a large, late avalanche results in a final red line that shows a small amount of concavity near its upper end. The effect of the avalanche is to steepen the upper part of the scree (between 10 and 20m in the horizontal), remove the convex region between 25m and 40m, and reduce the slope angle between 30m and 80m. The results are that an accumulated bump of material in the 20-40m region is redistributed along the scree, the slope is decreased overall, and an upper concavity is created that would in due course be filled by further rockfall.

Although the slope of the debris varies throughout the runs (and there is no systematic increase in slope towards the angle of repose through the evolution, as Statham (1973) inferred), the final mean slope does show some systematic behaviour as a function of the internal friction angle. Figure 7 shows the correlation between the two, along with the best linear fit to a scatter that hints at being asymptotic. Although the relationship is significant, the dependency is so weak that the largest final slope is less than 21º, even though this has a particle internal friction angle of over 50º. No significant relationships seemed to be present between the final slope and other model parameters.

5.4)Form of the rock-head

We can test the agreement of our simulations with the expressions of section 3, using the initial cliff-face angle $\beta=90^{o}$, but we require values of fractional expansion of debris, c,

angle of repose, α and height, h to do so. In these simulations, the value of c is generally very near zero, or even slightly negative (indicating that the debris is a little more compact than the original material). This reflects the way the original "rock" volume is constructed by dropping particles into a box – it is not representative of real rock bulk densities, and values of c are not physically meaningful. Furthermore, since the debris slope in our simulations is decreased by the sliding process, the cliff height, h, required in the above expressions to match the simulated rock core needs to be increased. A sample comparison is shown in Figure 8. It seems that the simulated shape of the rock core is quite a good fit to the original Fisher expressions provided that an effective cliff height of about 50m is used. The Fisher-Lehmann and Bakker-Le Heux expressions also fit reasonably, although they tend to have more curvature at the scree toe than in the simulations.

5.5)Size segregation

Figure 9 shows that there is appreciable evidence of size segregation in the later stages of the evolution. Plotted here is the mean size of the particles in 2m-wide horizontal bins smoothed with a top-hat filter of width 5m. This shows a progressive increase in size of just under 10%, from below the overall particle mean to above it, with distance along the slope away from the cliff (although the separation is not easy to discern by eye in Figure 4 for example). The size distribution of particles seems to have little effect on the segregation other than to lower the overall mean size – the change in size along the slope appears to have the same approximately linear behaviour for each distribution. However, there seems to be an additional effect for very high coefficients of restitution (greater than 0.7) as shown by the dashed line in Figure 9. As it happens these very high coefficients all correspond to the inverse-r distribution, but the other inverse r runs show similar behaviour to the other size distributions. Here it seems that in the very early part of the run the high degree of disturbance from falling material (cf Figure 3c – higher coefficient of

restitution is correlated with higher frequency of large events) results in a degree of homogenization of the size distribution. As the run progresses, this disturbed material is pushed out to the cliff foot, whereas the material in the upper part of the slope (horizontal position less than 55m) is processed through the later sliding mechanism and shows down-slope coarsening, as for the other runs.

6) Discussion

The dynamics of scree development can be discussed in terms of three interacting aspects:

1)Disaggregation and failure of the cliff surface

In this paper we have not examined in any detail the modes of cliff surface failure. Utili and Crosta (2011) further point out that the details of any effects of protection of the rock surface where there is overlying debris remain little examined: in reality there may be processes that would allow the buried lower part of the cliff face to be subject to degradation, depending on the properties of the rock and the porosity of overlying scree.

2)Form of the resulting rock core

If the buried material can loosen and become subject to movement this might affect possible rock core shapes. However, given we have assumed this is not the case, the analytic Fisher, Fisher-Lehmann and Bakker-Le Heux results seem to be reasonable approximate descriptions of its surface shape. For our model runs the original Fisher quadratic seems to provide the best fit to the final shape of the undisturbed rock, even though the exposure of the cliff face to weathering varies over time as the scree develops. However, the shape depends on the final mean slope angle of the scree, and is thus controlled by the behaviour of the debris.

3)Behaviour of the debris at the cliff foot

Most of the analytic models of scree development envisage a gradual build-up of debris falling from the cliff face in a series of infinitesimally thin layers. In these models the

slope below the cliff is linear, and in equilibrium at the angle of repose. An exception is the work of Caine (1969) in which Alpine slopes subject to slush avalanching are considered. However, the experiments of de Blasio and Saeter (2009) suggest that avalanching may be a common process in the development of the scree, and this is also the implication of our results (Figure 2): instead of a slow equilibrium development, the slope builds up in a series of accumulations followed by avalanches, where the latter have a size distribution that includes the whole length and a large fraction of the depth of the scree even in the later stages of development. Contrary to de Blasio and Saeter, however, we do not find that a weak layer of small particles is the cause of the avalanches; rather, it is a build-up of material in the upper portion of the scree that causes the slope to become unstable, and can then set nearly the whole volume of loose material in motion. Large slides lead to a stratigraphy in which "layers" of material are stretched almost horizontally in the lower parts of the slope, with the most recently weathered material higher up the scree and the oldest outcropping at the bottom, where the infinitesimal-build-up model would imply layers parallel to the scree surface at the angle of repose, with older (i.e. earliest weathered) material completely buried by younger (see e.g. Hutchinson 1998).

The early distribution of the avalanche events does not follow the power-law type behaviour that would be expected from the classic sand pile model for self-organised critical systems, although the later distribution lies close to a power law with slope near to -1.4 (cf fig 4b), rather similar to Bak et al's original 2D result (1987). However the system differs from the classic set up: there is a continuous decrease in the input energy of the particles, the input position systematically retreats over time, and the support of the system (by the underlying rock core) also changes form. So it is not surprising that the initial event distribution is not the same as an unsupported sand pile lying on a planar surface with fixed particle input energy. However field evidence from talus deposits (see e.g.

Hinchliffe and Ballantyne 2009, Sass 2006, Lewkowicz and Hartshorn,1998), provide some indication that a long-tailed distribution of event sizes is not unrealistic.

One aspect of the self-organised critical argument that seems to apply to the slopes we have modelled is that the final slope angle, slope curvature, size segregation, and event size distribution all appear to be largely independent of the individual particle properties, including the coefficient of restitution, particle size distribution and angle of internal friction. The effective (macroscopic) friction operating in column collapse simulation seems to show a similar low dependence on particle-scale friction angle for high values of friction coefficient (see e.g. Mangeney et al 2006), although we note that we have not examined in much detail whether there could be a sensitivity in the results to changes in maximum particle size, or the ratio of particle size to cliff height.

The values of slope angle that we find, though, are rather smaller than those that seem to emerge in the field. The rotation-suppressed disk models of Utili and Crosta (2011) lead to slope angles nearer to typical field values of 30º. On the one hand, experiments and simulations by Lacaze et al (2008) show that low slope angles can be obtained for real spherical particles, with reasonably good agreement between experiment and a direct simulation of the same geometry, with results that seem consistent with ours. On the other hand, Zenit (2005) suggests that low angles may be may in fact a result of lowering the dimensionality of the system to 2D. Utili and Crosta worry that the microscopic properties of the material, specifically the sliding and rolling friction coefficients, may need to be understood in greater detail before the debris dynamics can be understood. However, since even very high internal friction angles in our experiments, where rotation is allowed, do not reproduce their results, the implication is that a major control on slope angle is in fact either the particle and/or the simulation *geometry*. In practice, of course, irregular particles can in general rotate, so further work modelling such systems with more realistic particle

shapes is required in order to understand the slope evolution in more detail. Since irregular particles are more inclined to lock together, the expectation may be that the large scale avalanches seen here might be suppressed.

As for particle size segregation on the scree surface, Kirkby and Statham (1975) envisaged an essentially static slope on which boulders bounding down the surface would come to rest in a region in which they met with particles of a similar size. In our runs this mechanism seems to be absent, for two reasons: (i) few if any particles are able to propagate the full length of the slope in a single descent, even with coefficients of restitution as high as 0.9; and (ii) the particles tend to be stopped by surface variability that depends both on the particle size and the particle distribution. That is, small particles are able to trap larger ones in hollows or behind elevated clusters with sizes comparable to or larger than the largest particles (see e.g. the surface distribution of particles in Figure 4). The main mechanism for size segregation in these simulations seems to be the repeated avalanching process. As the particles move down the face of the scree, small gaps successively open and close in the structure, allowing the small sized particles to drop down, and leaving larger particles at the upper surface. The small particles are thus buried below the surface, and are thus also trapped in the upper reaches of the scree. This segregation mechanism is a well known aspect of this type of particle system (see e.g. Gray and Hutter 1997).

Simulations such as those reported here could inform field investigations, for example, designed to compare the stratigraphies of the upper and lower parts of the scree to establish if there is a gradual change from surface-parallel to near-horizontal surfaces, and to examine whether there is a down-slope increase in the degree of rock weathering. Use of ground-penetrating radar can give information about internal structure (see e.g Sass 2006), and laser scanning of surfaces could allow for large-scale systematic survey of

slope angles. However, the difficulty of obtaining reliable time series information from the field suggests that further experimental work to understand the build-up phase of a scree slope and the transition to a later regime with a long-tailed mass-movement distribution would be helpful, and could illuminate the history of events in a way difficult to validate otherwise

The fact that some of the largest scree avalanche events seem to occur when the scree is nearly mature implies that scree systems that still experience active rock-fall but appear to be stable may actually be prone to large-scale failure. In areas where triggering of debris flows may result from human disturbance (cf. Lorente et al 2002) there is a possibility that large slides could be set off inadvertently on mature slopes that are otherwise perceived as stable. Where such screes are at the head of an incline this may mean that they could pose a significant hazard, as such an event could lead to an extended debris flow. However, on flat surfaces the hazard is likely to be limited except on or very close to the scree, as the angle of repose seems to be limited to 17º even for spherical particles, at least in dry conditions. Roads and buildings at the base of mature scree could be at risk if a major slide occurs. Understanding the dynamics of the debris is thus potentially more important than studying failure modes of underlying rock surfaces when the cliff face is relatively stable and well consolidated, but still subject to rock-fall.

7) Conclusions

The evolution of the loose debris at the foot of scree slopes may be more complex than has previously been considered. Large rock slides appear to be able to take place at any stage of the evolution. This seems to be a robust property of our simulations, and seems to only depend weakly on internal properties of rock fragments. However, final slopes seem to be rather shallower than would be expected from field observations, independent of particle internal friction angle, and it may be that use of irregular particle shapes would

lead both to lower avalanche frequencies and steeper debris slopes. Further experiments involving non-spherical particle geometry, broader size distributions and fully three-dimensional dynamics need to be undertaken in order to shed more light on the evolution, particularly with regard to slope angle and curvature, and to clarify what aspects of the simulations presented here might be realistic.

8) Acknowledgements

Paul Cleary is thanked for invaluable discussions at an early stage in the development of this research.

This work was performed using the Darwin Supercomputer of the University of Cambridge High Performance Computing Service (http://www.hpc.cam.ac.uk/), provided by Dell Inc. using Strategic Research Infrastructure Funding from the Higher Education Funding Council for England. Discrete element simulations were parallelized using the CUDA Thrust library.

8) References

Bak P, Tang C, Wiesenfield K. 1987. Self-organized criticality: An explanation of 1/f noise. *Physical Review Letters* **59**: 381-384.

Bakker JP, Le Heux, JWN. 1952a. A Remarkable new Geomorphological Law I & II. *Koninkl. Nederl. Akademie van Wetenschappen* **55**: 399-571.

Bakker JP, Le Heux JWN. 1952b. Theory of Parallel Rectilinear Slope-Recession I & II. *Koninkl. Nederl. Akademie van Wetenschappen* **55**: 115-129.

Bakker JP, Le Heux JWN. 1947a. Theory on central rectilinear recession of slopes. I. *Koninkl. Nederl. Akademie van Wetenschappen* **50**: 959-956.

Bakker JP, Le Heux JWN. 1947b. Theory on central rectilinear recession of slopes. II.

Koninkl. Nederl. Akademie van Wetenschappen **50**: 1154-1162.

Bobet A, Fakhimi A, Johnson S, Morris J. 2009. Numerical Models in Discontinuous Media: Review of Advances for Rock Mechanics Applications. *Journal of Geotechnical* **135**: 1547.

Brockbank R, Huntley JM, Ball RC. 1997. Contact force distribution beneath a three-dimensional granular pile. *Journal de Physique II* **7**: 1521–1532.

Caine N. 1969. A Model for Alpine Talus Slope Development by Slush Avalanching. *The Journal of Geology* **77**: 92-100.

Calvetti F, Crosta G, Tatarella M. 2000. Numerical simulation of dry granular flows: from the reproduction of small-scale experiments to the prediction of rock avalanches. *Rivista Italiana di Geotecnica* **2**: 21–38.

Carson MA. 1977. Angles of repose, angles of shearing resistance and angles of talus slopes. *Earth Surface Processes* **2**: 363-380.

Cleary PW, Prakash M. 2004. Discrete-element modelling and smoothed particle hydrodynamics: potential in the environmental sciences. *Phil. Trans. Roy. Soc.* **362**: 2003-2030.

Cundall PA. 1971. A computer model for simulating progressive large scale movements in blocky rock systems. *Proc., Symp. of the Int. Society of Rock Mechanics* **1**: 129–36.

Cundall PA, Strack ODL.1979. A discrete numerical model for granular assemblies. *Geotechnique* **29**: 47–65.

De Blasio FV, Sæter M-B. 2009. Small-scale experimental simulation of talus evolution. *Earth Surface Processes and LandForms* **34**: 1685-1692.

Dickinson E, Milne SJ, and Patel M. 1989. Ordering in simulated packed beds formed

from binary mixtures of particles in two dimensions: implications for ceramic processing. *Powder technology* **59**: 11-24.

Durda DD, Movshovitz N, Richardson DC, Asphaug E, Morgan A, Rawlings AR Vest C. 2011. Experimental determination of the coefficient of restitution for meter-scale granite spheres. *Icarus* **211**: 849-855

Fisher O. 1866. On the disintegration of a chalk cliff. *Geological Magazine* **3**: 354-356.

Gray JMNT, Hutter K. 1997. Pattern formation in granular avalanches. *Continuum Mechanics and Thermodynamics* **9**: 341–345.

Hinchliffe S, Ballantyne CK. 2009. Talus structure and evolution on sandstone mountains in NW Scotland. *The Holocene* **19**: 477-486.

Hutchinson JN. 1998. A small-scale field check on the Fisher–Lehmann and Bakker–Le Heux cliff degradation models. *Earth Surface Processes and Landforms* **23**: 913-926.

Kirkby MJ, Statham I. 1975. Surface stone movement and scree formation. *The Journal of Geology* **83**: 349-362.

Lacaze L, Phillips JC, Kerswell RR. 2008. Planar collapse of a granular column: Experiments and discrete element simulations. *Physics of Fluids* **20**: 063302-1-12.

Lewkowciz A G Hartshorn J. 1998. Terrestrial record of rapid mass movements in the Sawtooth Range, Ellesmere Island, Northwest Territories, Canada. *Canadian journal of Earth Sciences* **35**: 55-64.

Lorente A JM, Beguería S, Arnáez J. 2002. Factors Explaining the Spatial Distribution of Hillslope Debris Flows. *Mountain Research and development* **22**: 32-39.

Luding S. 1997. Stress distribution in static two-dimensional granular model media in the absence of friction. *Physical Review E* **55**: 4720-4729.

Makse H, Johnson D, Schwartz L. 2000. Packing of compressible granular materials. *Physical review letters* **84**: 4160-3.

Mangeney A, Staron L, Volfson D, Tsimring L. 2006. Comparison between discrete and continuum modeling of granular spreading. *WSEAS Transactions on Mathematics* **2**: 63-70.

Munjiza A. 2004. The Combined Finite Discrete Element Method. John Wiley and sons, London. 333pp.

Nash D. 1981. FAULT: A FORTRAN program for modeling the degradation of active normal fault scarps. *Computers and Geosciences* **7**: 249-266.

Richards KS Dove M. (eds) 2004. Discrete-element modelling: methods and applications in the environmental sciences. *Phil. Trans. Roy. Soc*. **362**: 1795-2030.

Sass O. 2006. Determination of the internal structure of alpine talus deposits using different geophysical methods (Lechtaler Alps, Austria). *Geomorphology* **80**: 45-58.

Sass O, Krautblatter M. 2007. Debris flow-dominated and rockfall-dominated talus slopes: Genetic models derived from GPR measurements. *Geomorphology* **86**: 176-192.

Schäfer J, Dippel S, and Wolf DE. 1996. Force Schemes in Simluations of Granular Materials. *J. Phys. I France* **6**: 5-20

Scheidegger AE. 1961. Mathematical Models of Slope Development. *Geological Society of America Bulletin* **72**: 37-50.

Statham I. 1973. Scree slope development under conditions of surface particle movement. *Transactions of the Institute of British Geographers* **59**: 41–53.

Statham I. 1976. A scree slope rockfall model. *Earth Surface Processes* **1**: 43-62.

Tuzun U, Baxter J, Heyes DM. 2004, Analysis of the evolution of granular stress-strain and voidage states based on Dem simulations, *Phil. Trans. Roy. Soc*. **362**: 1931-1951.

Utili S, Crosta GB. 2011. Modelling the evolution of natural cliffs subject to weathering : 2 . Discrete elements approach. *Journal of Geophysical Research* **116**: F01017, DOI:10.1029/2009JF001559.

van Steijn H. 2002. Long-term landform evolution: evidence from talus studies. *Earth Surface Processes and Landforms* **27**: 1189-1199.

Zenit R. 2005. Computer simulations of the collapse of a granular column. *Physics of Fluids* **17**: 031703-1-4

Tables

Table 1: Sets of run parameters

Run set number (32 runs per set)	Restitution	Internal Friction angle(degrees)	Tangential dissipation (fraction of normal)	Size distribution
1	0.1	20	0.	Uniform
2	0.2	32.5	0.1	Uniform
3	0.3	45	0.3	Uniform
4	0.7	57.5	0.5	Uniform
5	0.7	20	0.9	r^{-1}
6	0.8	32.5	0.7	r^{-1}
7	0.9	45	0.8	r^{-1}
8	0.4	57.5	0.2	r^{-1}
9	0.4	20	0.4	r^{-3}
10	0.6	32.5	0.2	r^{-3}
11	0.1	45	0.6	r^{-3}
12	0.2	57.5	0.9	r^{-3}

Figures

Figure 1: Initial set-up of particles for scree experiments, showing the random nature of the positions. Particles are coloured by size. The block of material on the left of the figure is initially locked in place. The ground surface to the lower right remains locked in position throughout. The initial cliiff height is approximately 45m and the depth of rock behind the cliff also approximately 45m

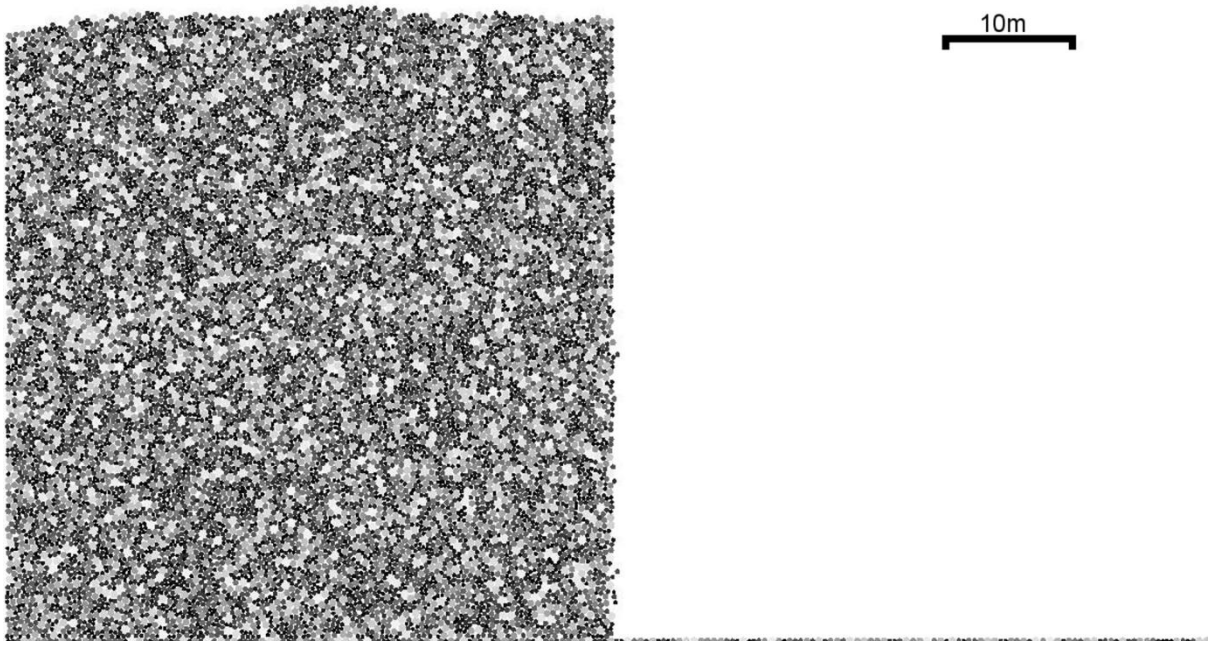

Figure 2: Time-series of the number of particles in the scree slope with velocities lying in the range 0.05ms^{-1} to 2 ms^{-1} for three runs of the model taken from run sets with different internal friction angles (a)57.5^{o} (set 4, run 3); (b)32.5^{o}(set 6, run 4); and (c)20^{o} (set 9, run 7). Runs show a high degree of variability, but have similar overall properties. Note that the maximum size of avalanches grows over time with the scree, but the fraction of loose particles in motion can be as high as 80% at any time (see Fig 4).

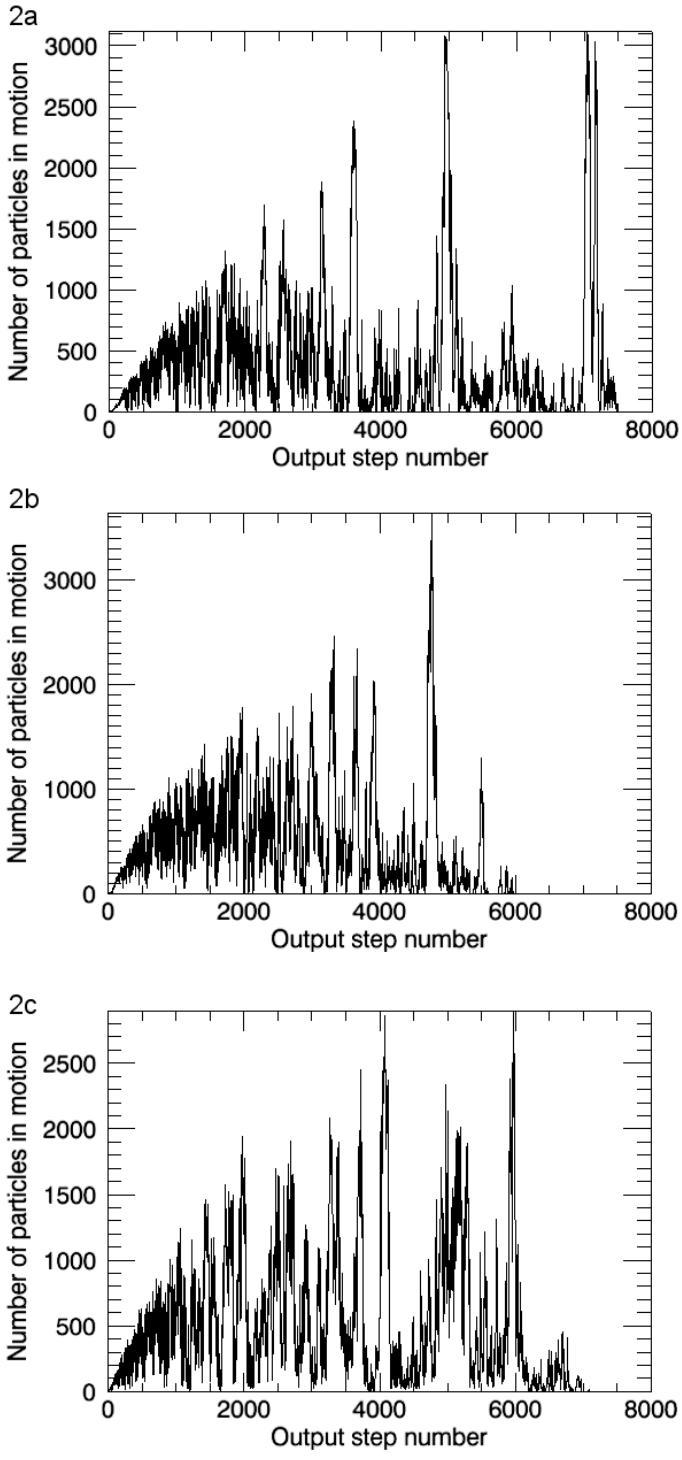

Figure 3: Size distribution of event peaks (a) prior to output step 1500 (b) after output step 1500. Bold curve shows the mean for run set 4 (cf fig 2a) with standard deviation from the 32 runs in the set. Lighter curves show the mean event size distributions for the other 11 run sets. (c) correlation of number of events at the maxima in (a) with coefficient of restitution.

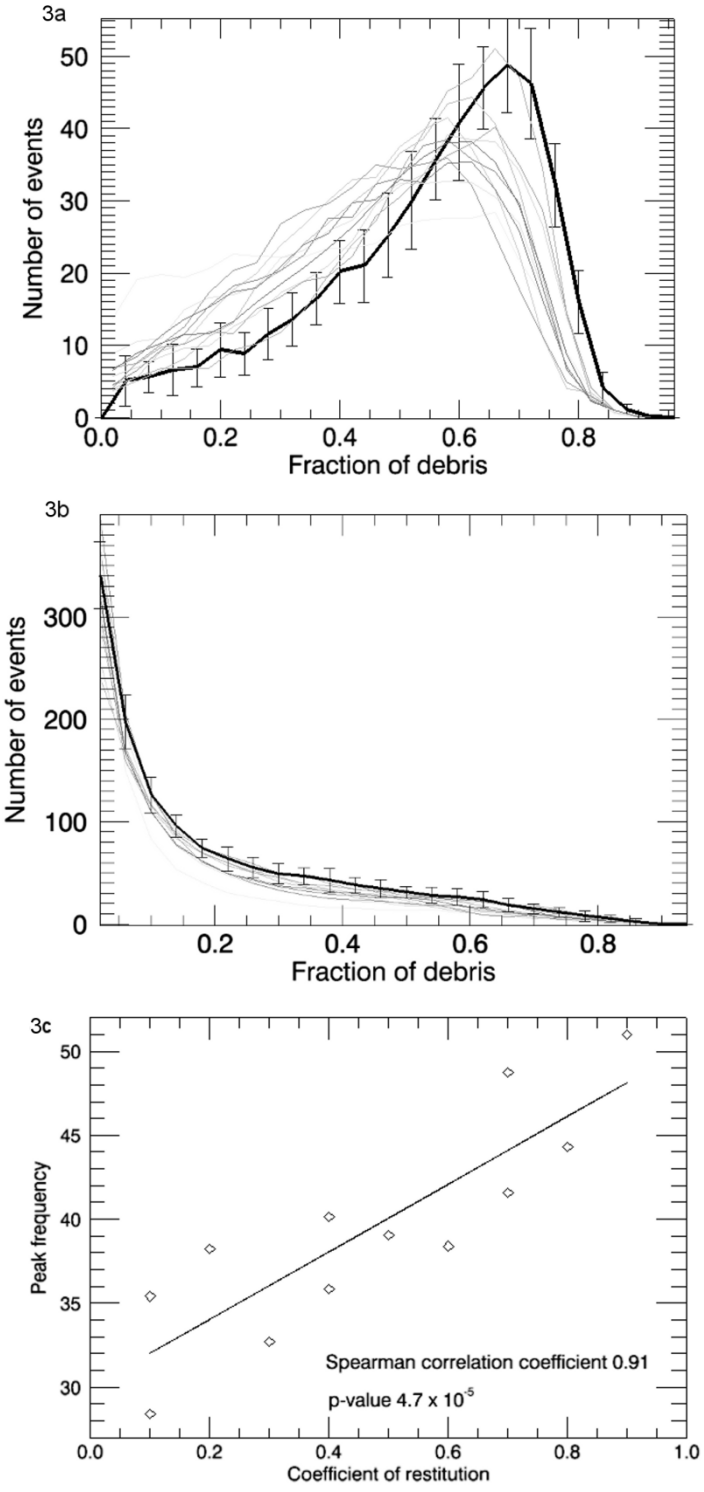

Figure 4: Velocity distribution near the peak of an avalanche event (output step 4763, Fig. 2b). Velocities of falling particles can reach up to 8m s^{-1} at this stage, but speeds in the scree are generally below 2m s^{-1}. At this stage almost all the scree is in motion except for the small area near the rock "nose" with lower velocities near the base, velocity contours being more or less aligned with the scree surface slope.

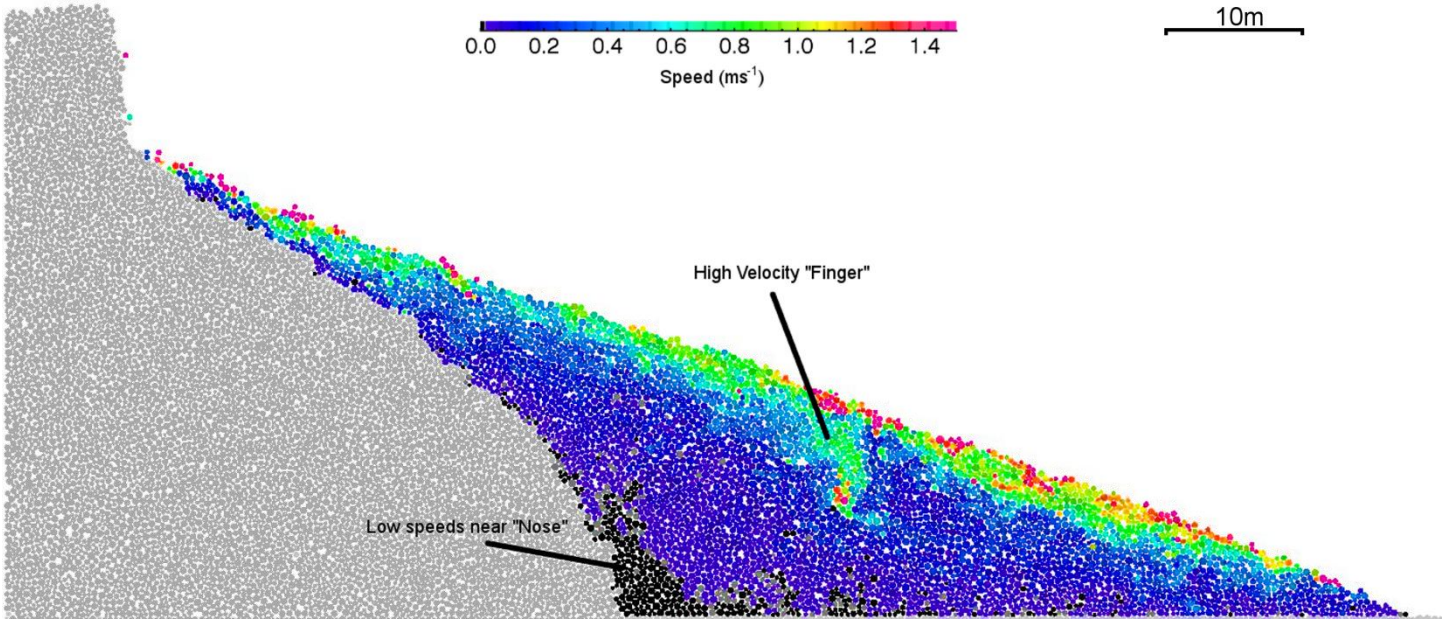

Figure 5: View of the final state for run set 9 run 7 (figure 2c) coloured with initial horizontal position. To the left the vertical bands of colour show the regions where material has not moved (cf figure 4) and material in the scree has the same colour scheme, showing where material in the debris originated in the original cliff face. Material in the debris shows near-horizontal layering, with a slope significantly less than the surface, reflecting a combination of shearing during avalanches and limited down-slope propagation.

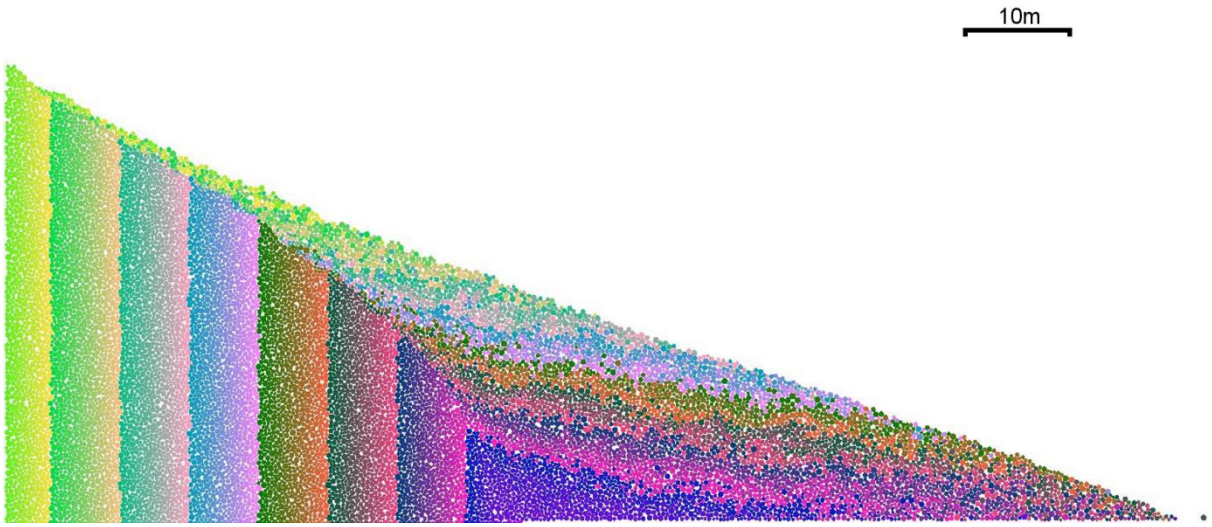

Figure 6: Time series showing evolution of the scree surface in set 9 run 27. Each line is separated from the next by 250 output time units, with blue denoting earlier times and red colours later. Position of the surface is represented by the mean of the highest three particles positions in bins of horizontal width 2m. Stars show some weak tendency toward benching near the cliff at early stages. Slopes at intermediate times have a rather straight profile (plus signs). Diamonds show that the slope is steeper at output step near 6000 than later, owing to a large late avalanche in this run.

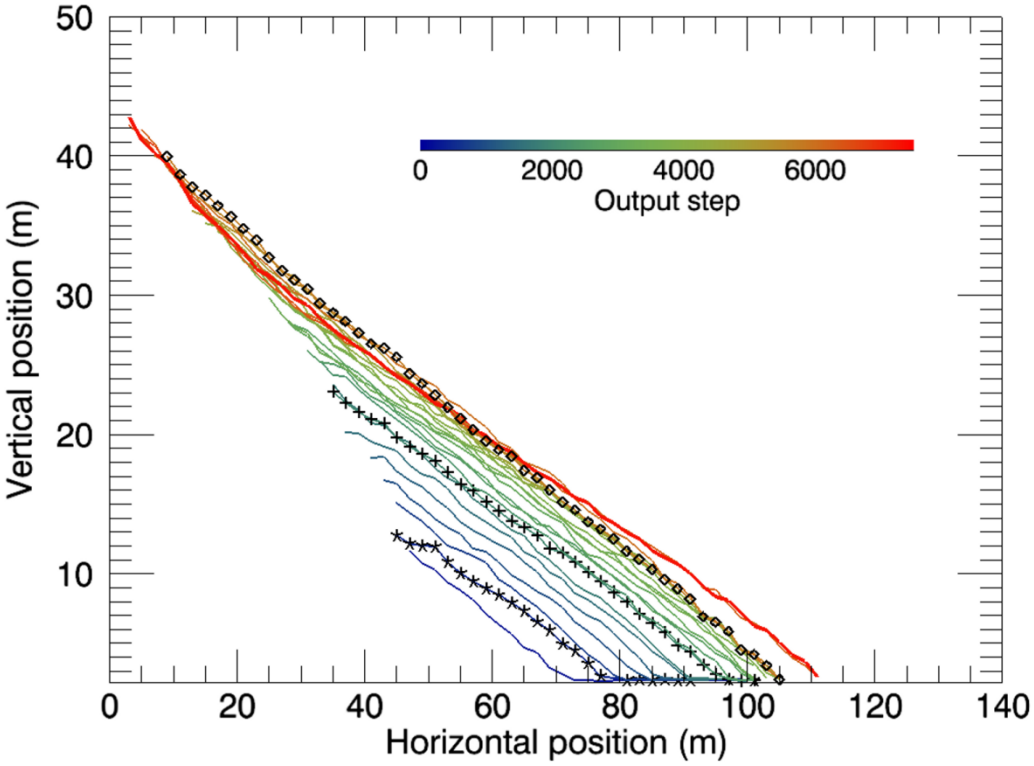

Figure 7: Final mean slope of the debris surface for each run set plotted against internal friction angle, with correlation coefficient and best fit line.

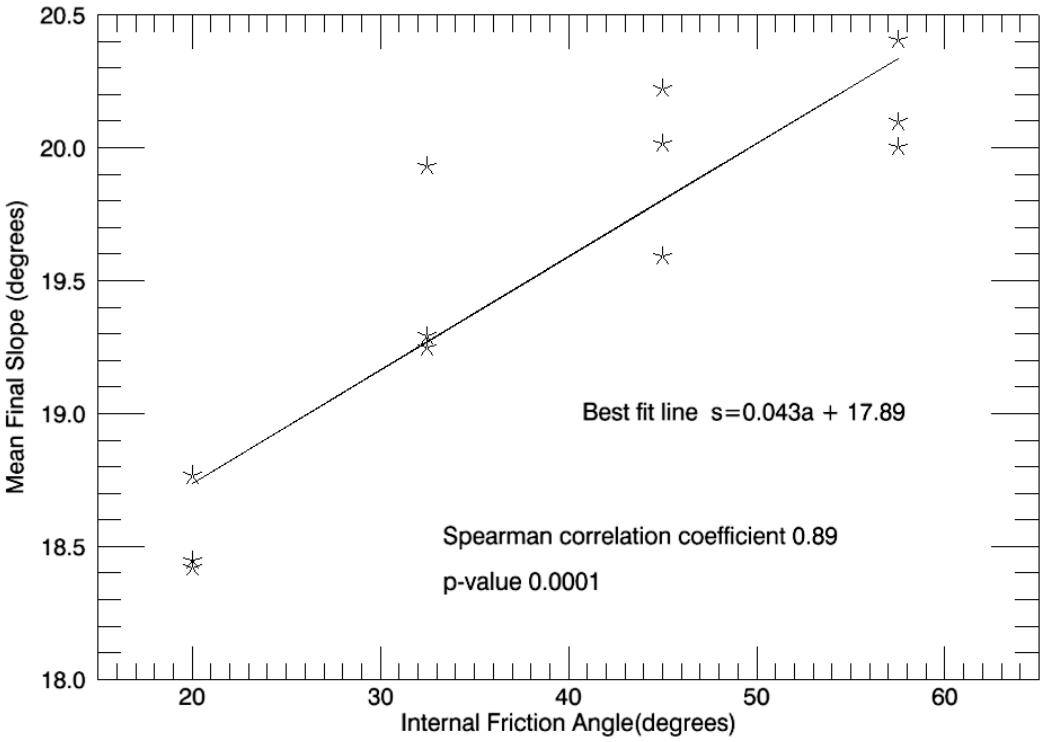

Figure 8: Final rock-core for set 5 run 1 estimated using the highest points in bins of width 2m (black dotted line), plotted with the predictions of the Fisher-Lehmann(green, χ^2 4.46, p-value 9.6×10^{-6}) Bakker- Le Heux (blue, χ^2 6.88, p-value 4.7×10^{-4}) and original Fisher quadratic (red, χ^2 2.82, p-value 10^{-7}), using an effective cliff height of 49m. Other runs show similar results.

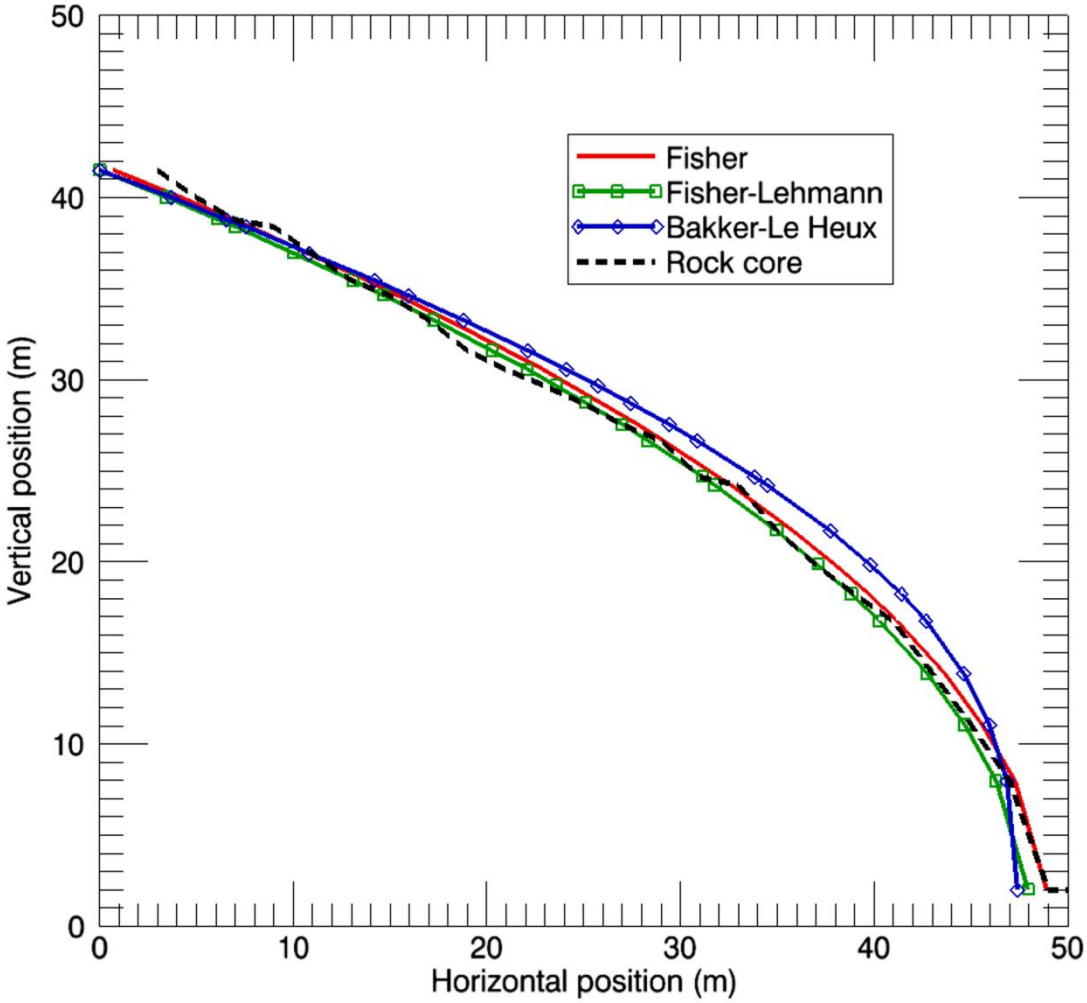

Figure 9: Particle-size distributions down the length of the scree slope at the end of the model runs. Mean size of particles in bins of width 2m are shown. The upper line show the mean of 32 runs from set 1, which has a uniform size distribution. The lower line shows the mean for run set 12 (distributed as r^{-3}), also showing the standard deviation – variability is comparable for the other runs, but the error bars are omitted for clarity. The dot-dashed line shows the mean for run set 8 (low coefficient of restitution) and the dashed line that for run set 7 (high coefficient of restitution), both of which have particle sizes distributed as r^{-1}.